



## Enhanced CO<sub>2</sub> photocatalytic reduction on alkali-decorated graphitic carbon nitride



Zhuxing Sun <sup>a,b,c,1</sup>, Julia Melisande Theresa Agatha Fischer <sup>d,1</sup>, Qian Li <sup>a,b</sup>, Jing Hu <sup>a,b</sup>, Qijun Tang <sup>a,b</sup>, Haiqiang Wang <sup>a,b,\*</sup>, Zhongbiao Wu <sup>a,b</sup>, Marlies Hankel <sup>d</sup>, Debra J. Searles <sup>d,e</sup>, Lianzhou Wang <sup>c,\*\*</sup>

<sup>a</sup> Key Laboratory of Environment Remediation and Ecological Health, Ministry of Education, College of Environmental & Resources Science, Zhejiang University, Hangzhou 310058, PR China

<sup>b</sup> Zhejiang Provincial Engineering Research Center of Industrial Boiler & Furnace Flue Gas Pollution Control, Hangzhou, 311202, PR China

<sup>c</sup> Nanomaterials Centre, School of Chemical Engineering and Australian Institute for Bioengineering and Nanotechnology, The University of Queensland, Brisbane, QLD 4072, Australia

<sup>d</sup> Australian Institute of Bioengineering & Nanotechnology, The University of Queensland, QLD 4072, Australia

<sup>e</sup> School of Chemistry and Molecular Biosciences, The University of Queensland, QLD 4072, Australia

### ARTICLE INFO

#### Article history:

Received 16 February 2017

Received in revised form 11 May 2017

Accepted 22 May 2017

Available online 24 May 2017

#### Keywords:

CO<sub>2</sub> conversion

Photocatalysis

g-C<sub>3</sub>N<sub>4</sub>

Alkali

DFT calculations

### ABSTRACT

In this work, visible-light photocatalytic reduction performance of carbon dioxide (CO<sub>2</sub>) on graphitic carbon nitride (g-C<sub>3</sub>N<sub>4</sub>) was significantly promoted by the decoration of potassium hydroxide (KOH) on g-C<sub>3</sub>N<sub>4</sub>. More importantly, the role of KOH was thoroughly discussed via various characterizations, control experiments and density functional theory (DFT) calculations. It was found that KOH decoration did not result in any significant difference regards to the morphology, elemental states, BET surface area and light adsorption of g-C<sub>3</sub>N<sub>4</sub> except a drastically enhanced CO<sub>2</sub> adsorption capacity. The promotion effect of KOH on g-C<sub>3</sub>N<sub>4</sub> was mainly contributed by the hydroxide ion (OH<sup>-</sup>) functioning as both a hole accepter and a driving force to keep a dynamically stable amount of H<sub>2</sub>CO<sub>3</sub> (probably the major form of CO<sub>2</sub> to be reduced) on the surface of the catalyst. Moreover, the different extents of influence of NaOH and KOH on g-C<sub>3</sub>N<sub>4</sub> were revealed and further explained using computational results. This study supplements current understanding on alkali-promoted photocatalytic processes and provides new insights into the mechanism of CO<sub>2</sub> photocatalytic reduction.

© 2017 Published by Elsevier B.V.

### 1. Introduction

Photocatalytic reduction of carbon dioxide (CO<sub>2</sub>) into fuel (methane, methanol, carbon monoxide etc.) with water as reducing agent is a green technology that aims to mimic the photosynthesis process in nature and has attracted increasing attention in the past few decades [1–7]. The major challenge and focus of studies in this area is the development of an efficient, stable

and cost-effective photocatalyst. Over the past four decades, various semiconductor photocatalysts including metal oxides (TiO<sub>2</sub> [8], Cu<sub>2</sub>O [9], CeO<sub>2</sub> [10,11]); oxysalts (KTaO<sub>3</sub> [12], Bi<sub>2</sub>WO<sub>6</sub> [13] etc.), metal chalcogenides (ZnS [14], Bi<sub>2</sub>S<sub>3</sub>, [15] etc.), and non-metal materials (graphene oxide [16], carbon nitride [17], etc.) have been studied for photocatalytic conversion of CO<sub>2</sub>. Among them, graphitic carbon nitride (g-C<sub>3</sub>N<sub>4</sub>), has gained tremendous attention recently as an easily-obtained, low-cost and visible-light-responsive non-metal semiconductor photocatalyst that shows great stability and non-toxicity [7,18–25].

There have been several pioneering reports on the use of g-C<sub>3</sub>N<sub>4</sub> for CO<sub>2</sub> photocatalytic reduction [20,21]. The CO<sub>2</sub> photocatalytic reduction on g-C<sub>3</sub>N<sub>4</sub> was successfully enhanced by forming heterojunctions or Z-scheme structures with other semiconductors such as In<sub>2</sub>O<sub>3</sub> [26], NaNbO<sub>3</sub>, Bi<sub>2</sub>WO<sub>6</sub> [27], [28] BiVO<sub>4</sub> [29], Ag<sub>3</sub>PO<sub>4</sub> [30], BiOI [31], LaPO<sub>4</sub> [32], ZnO [33,34], CeO [35] and AgBr/graphene [36]. These improvements were mainly due to the promoted separation and transfer of photo-generated electrons and holes, addressing

\* Corresponding author at: Key Laboratory of Environment Remediation and Ecological Health, Ministry of Education, College of Environmental & Resources Science, Zhejiang University, Hangzhou, 310058, PR China.

\*\* Corresponding author at: Nanomaterials Centre, School of Chemical Engineering and Australian Institute for Bioengineering and Nanotechnology, The University of Queensland, Brisbane, QLD 4072, Australia.

E-mail addresses: [haiqiangwang@zju.edu.cn](mailto:haiqiangwang@zju.edu.cn), [wanghaiqiang2008@126.com](mailto:wanghaiqiang2008@126.com) (H. Wang), [l.wang@uq.edu.au](mailto:l.wang@uq.edu.au) (L. Wang).

<sup>1</sup> These authors contributed equally.

one of the major drawbacks of  $\text{g-C}_3\text{N}_4$ . Another major problem in using  $\text{g-C}_3\text{N}_4$  for photocatalytic  $\text{CO}_2$  reduction is its limited ability to adsorb/activate  $\text{CO}_2$ . But this issue is usually less emphasized. Amine functionalization [37] and UIO66 [38] (a type of metal organic framework) have been applied to enhance  $\text{CO}_2$  adsorption on  $\text{g-C}_3\text{N}_4$  in order to achieve superior  $\text{CO}_2$  conversion. This suggests that increasing the amount of adsorbed  $\text{CO}_2$  is an effective method to enhance  $\text{CO}_2$  photocatalytic reduction on  $\text{g-C}_3\text{N}_4$ .

Recently, the alkaline earth metal oxide,  $\text{MgO}$  [39–42], and the alkali,  $\text{NaOH}$  [43], have been reported to be able to enhance  $\text{CO}_2$  photocatalytic conversion on  $\text{TiO}_2$ . The positive influences were attributed to an enhanced  $\text{CO}_2$  activation and, probably more importantly, a facilitated oxidation process. However, a detailed understanding of the overall mechanism is lacking.

In this work,  $\text{KOH}$  was decorated on  $\text{g-C}_3\text{N}_4$  and a 3-fold enhancement in production of carbon monoxide (CO), methane ( $\text{CH}_4$ ) and acetaldehyde ( $\text{CH}_3\text{CHO}$ ) from photocatalytic reduction of  $\text{CO}_2$  was observed. To understand the role of  $\text{KOH}$ , detailed characterizations, control experiments, and DFT calculations were carried out. The difference between  $\text{KOH}$  and  $\text{NaOH}$  were also discussed to emphasize the important influence of the cations on the photocatalytic reduction performance.

## 2. Experimental

### 2.1. Sample preparation

All chemicals were analytically pure and used without further treatment. Graphitic carbon nitride ( $\text{g-C}_3\text{N}_4$ ) was synthesized by heating 30 g of urea in a 100 ml crucible with a cover in static air at 550 °C for 2 h with a ramping rate of 10 °C min<sup>−1</sup>. We refer to this sample as CN.

$\text{KOH}$  and  $\text{NaOH}$  were deposited on  $\text{g-C}_3\text{N}_4$  by simply impregnating 0.6 g of  $\text{g-C}_3\text{N}_4$  in aqueous solution with various quantities of  $\text{KOH}$  (0.05, 0.1, 0.25, 0.5, 1.0 wt%) or  $\text{NaOH}$  (0.5, 1.0, 2.0, 3.0 wt%). The suspensions were sonicated and stirred to fully disperse the  $\text{g-C}_3\text{N}_4$  and then dried in a rotary evaporator. Finally, the dried sample was recollected and ready for use. The samples were denoted as xKOH-CN (x = 0.05, 0.1, 0.25, 0.5, 1.0) and yNaOH-CN (y = 0.5, 1.0, 2.0, 3.0).  $\text{KCl}$ ,  $\text{KHCO}_3$  and  $\text{K}_2\text{CO}_3$  patched  $\text{g-C}_3\text{N}_4$  samples were also prepared in the same way.

### 2.2. Characterization methods

X-ray powder diffraction (XRD) patterns were recorded on an X-ray diffractometer (Model D/max RA, Japan) with  $\text{Cu K}\alpha$  irradiation. Fourier transform infrared (FTIR) spectra were obtained on an FTIR spectrometer (Bruker Alpha, Germany) equipped with a deuterated triglycine sulfate (DTGS) detector using sample discs prepared with dried KBr. X-ray photoelectron spectroscopy (XPS; Thermo ESCALAB 250Xi, USA) measurements were performed with a monochromatized  $\text{Al K}\alpha$  source (150 W, 500  $\mu\text{m}$ ,  $h\nu = 1486.6\text{ eV}$ ). The carbon 1 s line (284.8 eV) was used as the reference to calibrate the binding energies. Field emission scanning electron microscope (FE-SEM; Hitachi SU8020, Japan) and transmission electron microscope (TEM, Fei F20, USA, Voltage: 200 kV) were used to study the morphology of the samples. The Brunauer-Emmett-Teller (BET) specific surface area was calculated from the multipoint BET method on a physisorption analyzer (JW-BK 132F, Beijing JWGB Sci & Tech Co., China). The UV-vis diffuse reflection spectra (UV-vis DRS) were obtained on an UV-vis spectrophotometer (TU-1901, China) equipped with an integrating sphere assembly and  $\text{BaSO}_4$  was used as the reflectance. The photoluminescence spectra were measured with a fluorescence spectrophotometer (RAMANLOG 6, USA) using 420 nm lasers as excitation source. The photocurrent of

the samples at different pH was measured on an electrochemical workstation (CHI 660E, China) with 1.5 M  $\text{Na}_2\text{SO}_4$  as the electrolyte. The pH was tuned by addition of  $\text{KOH}$  or  $\text{NaOH}$ .  $\text{CO}_2$  adsorption tests were carried out on a thermo gravimetric analysis instrument (TGA, SDT Q600 V8.2 Build 100). The samples were pretreated with flowing He at 120 °C for 2 h and exposed to  $\text{CO}_2$  at 50 °C. The changes in weights during the process were recorded to value their  $\text{CO}_2$  adsorption capacities.

### 2.3. $\text{CO}_2$ photocatalytic reduction experiment

$\text{CO}_2$  photocatalytic conversion in the presence of  $\text{H}_2\text{O}$  was conducted in a homemade stainless-steel-made reactor with a quartz window on the top. The system was operated in a continuous-flow mode. For each test, 40 mg of catalyst was evenly dispersed at the bottom of the reactor. A 300 W Xeon lamp (PLS-SXE300UV, Beijing Trust-tech Co. Ltd, China) with a light filter was used to obtain visible light with wavelengths larger than 420 nm. (To note, the  $\text{CO}_2$  photocatalytic reduction experiments to compare the influence of anions in Section 3.3 were conducted under irradiation of the full spectrum of the Xeon light.) After the reactor was sealed,  $\text{CO}_2$  (99.9999%) was purged into the reactor through a water bubbler, delivering a gas mixture of  $\text{CO}_2$  and  $\text{H}_2\text{O}$ , at 120  $\text{ml}\cdot\text{min}^{-1}$  for 1 h in order to remove any impurity gases. Then the flow was maintained at 3.0  $\text{ml}\cdot\text{min}^{-1}$  for another 1 h to stabilize the system before the irradiation source was turned on. During the reaction, gaseous products in the reactor effluent were analyzed at certain time intervals using a calibrated gas chromatography (Agilent 7890A, USA) which was equipped with two flame ionization detectors (FID) and a thermal conductivity detector (TCD). The accumulated yields of the products were obtained by integrating the production rate over time. The samples after reaction were collected to check if there are any products attached on the surface by extraction with water and subsequent detection with GC (for hydrocarbons) and ion chromatograph (for formic acid mainly). Experiments without light irradiation, using  $\text{N}_2$  instead of  $\text{CO}_2$  and without addition of a catalyst, were also conducted and little product could be detected, indicating that the products are from the photocatalytic reduction of  $\text{CO}_2$ . In addition, isotope tracing experiments were also conducted using  $^{13}\text{CO}_2$  (99 atom% C, SIGMA-ALDRICH Co.) in a batch reactor and confirmed that the products are from  $\text{CO}_2$  rather than from any carbon-containing contaminants.

### 2.4. In situ DRIFTS experiments

In situ diffuse reflectance FT-IR spectroscopy (DRIFTS) was carried out on a Nicolet 6700 spectrometer (Thermo Electron) equipped with a liquid nitrogen cooled  $\text{HgCdTe}$  (MCT) detector, a Praying Mantis DRIFTS accessory and a reaction cell (Harrick Scientific, HVC-DRP). The reaction chamber is equipped with a heater and a temperature controller as well as a sample cup in the center. There are three windows on the dome of the cell: two  $\text{CaF}$  windows for IR transmission and a quartz window allowing transmission of irradiation light from a 300 W Xe lamp (PLS-SXE300UV, Beijing Trust-tech Co. Ltd, China). The spectra recorded were displayed in absorbance units and acquired with a resolution of 4  $\text{cm}^{-1}$ , using 32 scans.

After the sample was loaded in the reaction cell, the cell was purged with helium (He) at 30  $\text{ml}\cdot\text{min}^{-1}$  at 200 °C for 1 h to eliminate any absorbed gas on the surface of the sample and any impurity gases in the chamber. Then the cell was cooled down to 50 °C and the background spectrum was collected. Subsequently, a  $\text{CO}_2/\text{H}_2\text{O}$  mixture, delivered by passing  $\text{CO}_2$  through a water bubbler at 3  $\text{ml}\cdot\text{min}^{-1}$ , was introduced to allow absorption saturation. IR spectra were recorded as a function of time (0–60 min). To eliminate any physisorbed species, the system was purged with He again

for 30 min. Subsequently, the light was turned on and the system was irradiated for 120 min while the time-resolved IR spectra were collected to investigate chemical changes on the sample surface.

## 2.5. Computational methods

All calculations were performed with Vienna Ab Initio Simulation Package (VASP) [44] with periodic boundary conditions and projector-augmented wave (PAW) [44]. The generalized gradient approximation (GGA) with the Perdew-Burke-Ernzerhof (PBE) functional [45] and dispersion correction by Grimme (DFT-D2) [46] were used to describe the electronic structure. For the  $2 \times 2$  unit cell, the Brillouin zone was sampled by a  $3 \times 3 \times 1$  k-point mesh and a cutoff energy of 500 eV was used. The vacuum slab between two layers was set to 20 Å.

A positive binding energy ( $E_{bind}$ ) indicates stable adsorption at 0 K, and was calculated by the difference between the total energies of the surface with adsorbates ( $E_{SF+mol}$ ) and energies of the two separate systems (the surface  $E_{SF}$  and of the molecule  $E_{mol}$ ):

$$E_{bind} = -(E_{SF+mol} - E_{SF} - E_{mol}) \quad (1)$$

There are number of stoichiometrically equivalent structures of  $g\text{-C}_3\text{N}_4$  and here we consider the structure which comprises tri-s-triazine (also referred to as heptazine) units connect through graphitic nitrogen atoms to form a 2D sheet. Details on the preparations of the corrugated sheets, can be found in the Supporting information. To model the  $g\text{-C}_3\text{N}_4$  surface, we used a  $2 \times 2$  supercell of  $g\text{-C}_6\text{N}_8$  [47], with an optimized lattice constant of 13.59 Å for the corrugated sheets. Furthermore, to include the  $-\text{NH}$  bond, one of the tri-s-triazine units of  $g\text{-C}_6\text{N}_8$ -units was replaced by three hydrogen atoms, to saturate the three nitrogen dangling bonds. Both of these systems are shown in Fig. 1. The corrugation of the sheet was separately calculated and the optimized lattice constant for the  $-\text{NH}$  containing system was determined to be 13.83 Å.

## 3. Results and discussion

### 3.1. Physical and optical properties

The XRD patterns of CN, 0.1KOH-CN and 1.0KOH-CN are presented in Fig. 2a. All the samples show the characteristic diffraction peaks of typical  $g\text{-C}_3\text{N}_4$  at  $2\theta = 12.9^\circ$  and  $2\theta = 27.5^\circ$ . The strongest peak at  $2\theta = 27.5^\circ$  is indexed to the [002] plane with  $d = 0.326$  nm, a characteristic interlayer spacing of CN aromatic units. The peak at  $2\theta = 12.9^\circ$  is ascribed to the in-plane structural packing motif of tri-s-triazine units [19]. No new peaks or peak shifts are observed after KOH decoration. However, interestingly, the peak intensity increases with the amount of KOH. As all the samples were tested under the same conditions, the difference in peak intensity could not be attributed to measurement errors. This suggests that the impregnation of  $g\text{-C}_3\text{N}_4$  in KOH solution and the following evaporation process could have helped the  $g\text{-C}_3\text{N}_4$  form structures with enhanced ordering. Fig. 2b presents the FTIR spectra of the samples. All the samples show adsorption in the same ranges, i.e.  $810\text{ cm}^{-1}$  for the breathing mode of the tri-s-triazine units,  $1100\text{--}1650\text{ cm}^{-1}$  for typical stretching modes of heterocycles of carbon and nitrogen and broad adsorption at  $2700\text{--}3600\text{ cm}^{-1}$  from stretching vibration modes of  $-\text{NH}$  [48] without much difference, indicating that the loading of KOH cannot change the main functional groups of  $g\text{-C}_3\text{N}_4$ . And, due to the low amount of KOH, the FTIR peaks of KOH is too minor to be recognizable.

The morphology and microstructure of the samples were investigated by scanning electron microscope (SEM) and transmission electron microscope (TEM), as shown in Fig. 3. No apparent difference could be observed between CN and KOH-loaded CN. All

the samples show morphologies of curved porous sheets stacking together as commonly reported for  $g\text{-C}_3\text{N}_4$  synthesized from urea [49–52]. In addition, the BET surface areas calculated from  $\text{N}_2$  adsorption-desorption curves of the unmodified and all the KOH-decorated  $g\text{-C}_3\text{N}_4$  are very close to each other, as listed in Table 1. These indicate that the preparation processes have little influence to the macrostructure of  $g\text{-C}_3\text{N}_4$  and the limited amount of KOH should be deposited just on the surface of  $g\text{-C}_3\text{N}_4$ .

Subsequently, X-ray photoelectron spectroscopy (XPS) measurements were carried out to analyze the chemical states of the elements in the samples before and after KOH loading. Fig. 4 exhibits C 1s, N 1s, O 1s and VB XPS spectra of CN, 0.1KOH-CN and 1.0KOH-CN. The states of carbon, nitrogen and oxygen as well as the VB location changed little before and after KOH loading. The binding energy of K 2p is 292–295 eV but no peaks in this range are visible in the XPS spectra of 0.1KOH-CN and 1.0KOH-CN due to the low content of KOH in these samples.

The amount of oxygen in CN, 0.1KOH-CN and 1.0KOH-CN are estimated to be 5.6 at%, 8.1 at% and 12.1 at%, respectively based on peak areas in the XPS survey spectra. The oxygen could mainly consist of residual oxygen from the polymerization process of urea [49] and the oxygen from KOH. As the amount of the former form of oxygen should be consistent in all samples, the increased amount of oxygen is expected to be from the increased amount of deposited KOH. Besides, a peak due to K can be observed in the energy dispersive X-ray (EDX) test in SEM of the 1.0KOH-CN sample (Fig. 5) with the content estimated to be around 0.8 wt% (~1.48 at%), suggesting the successful decoration of KOH on the surface of  $g\text{-C}_3\text{N}_4$ .

$\text{CO}_2$  adsorption at 50 °C (Fig. 6) further verifies the successful loading of KOH on the sample surface. While CN only adsorbs 0.28 wt%  $\text{CO}_2$ , 0.65 wt%  $\text{CO}_2$  is adsorbed on 0.1KOH-CN and a further increase (0.9 wt%) is observed on 1.0 KOH-CN. As mentioned above, CN, 0.1KOH-CN and 1.0KOH-CN possess similar BET surface areas. The KOH deposited on  $g\text{-C}_3\text{N}_4$  is expected to be the only cause for the enhanced  $\text{CO}_2$  adsorption.

In terms of optical properties, KOH exerted little influence on the light absorption of  $g\text{-C}_3\text{N}_4$ . As demonstrated in Fig. 7a, all the  $g\text{-C}_3\text{N}_4$  samples without or with different amount of KOH show the same light adsorption ranges with the absorption edge at around 450 nm. Fig. 7b gives the photoluminescence (PL) spectra of CN, 0.1KOH-CN and 1.0KOH-CN. The peak locations of the three samples are alike. A small increase in intensity is observed as the KOH loading amount increases. This suggests that the addition of KOH slightly increases the recombination rate of photo-generated electrons and holes. However, this effect is too small for 0.1KOH-CN to cause any possible influence on the photocatalytic activity of  $g\text{-C}_3\text{N}_4$ .

### 3.2. $\text{CO}_2$ photocatalytic reduction on KOH-loaded $g\text{-C}_3\text{N}_4$

The 5-h productions in  $\text{CO}_2$  photocatalytic reduction under visible light ( $\lambda > 420$  nm) using CN and its corresponding samples with KOH decoration as photocatalyst are presented in Fig. 8 while the time-dependent data is provided in Fig. S1 (Supporting information). The products detected consist of  $\text{CO}$ ,  $\text{CH}_4$  and  $\text{CH}_3\text{CHO}$  and the detailed amounts of the compounds produced as well as the contributions of the whole  $\text{CO}_2$  converted are listed in Table S1 (Supporting information). Liquid products such as formaldehyde, methanol and ethanol were not detected in the current reaction system. As shown in Fig. 8, the productions of all the products increase a bit with the addition of 0.05 wt% KOH. When 0.1 wt% KOH is used, the productions improve greatly and become about 3 times those of CN. However, the  $\text{CO}_2$  conversion decreases as the amount of applied KOH increases further.

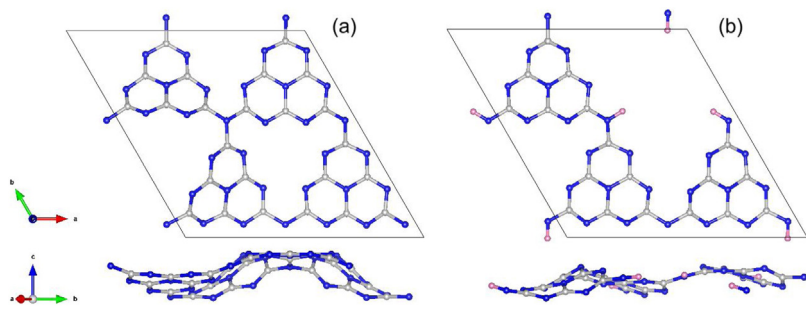


**Fig. 1.** Unit cell for  $\text{g-C}_3\text{N}_4$  (a) and  $-\text{NH}$  containing  $\text{g-C}_3\text{N}_4$  (b). (Grey – carbon atoms, blue – nitrogen atoms and pink – hydrogen atoms). (For interpretation of the references to colour in this figure legend, the reader is referred to the web version of this article.)

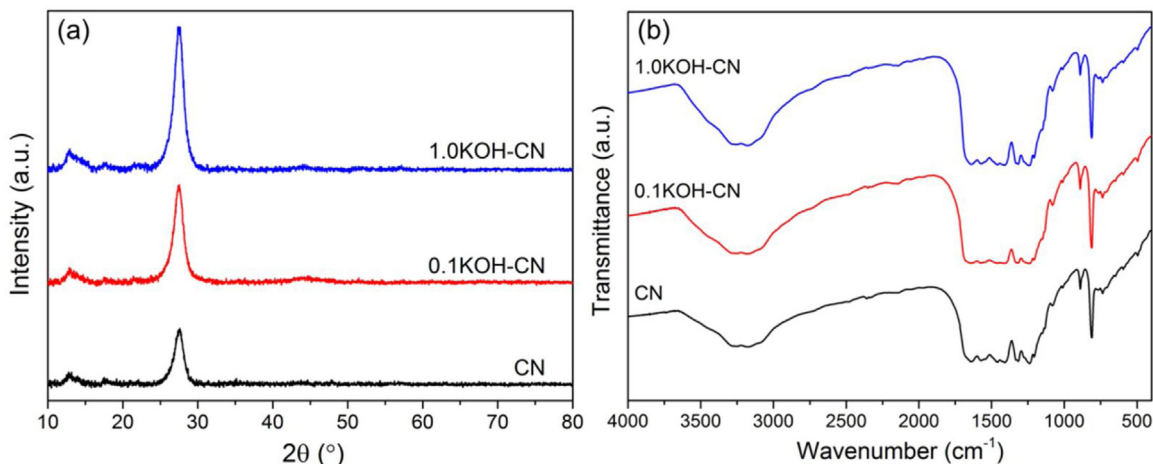


**Fig. 2.** XRD patterns (a) and FTIR spectra (b) of CN, 0.1KOH-CN and 1.0KOH-CN.

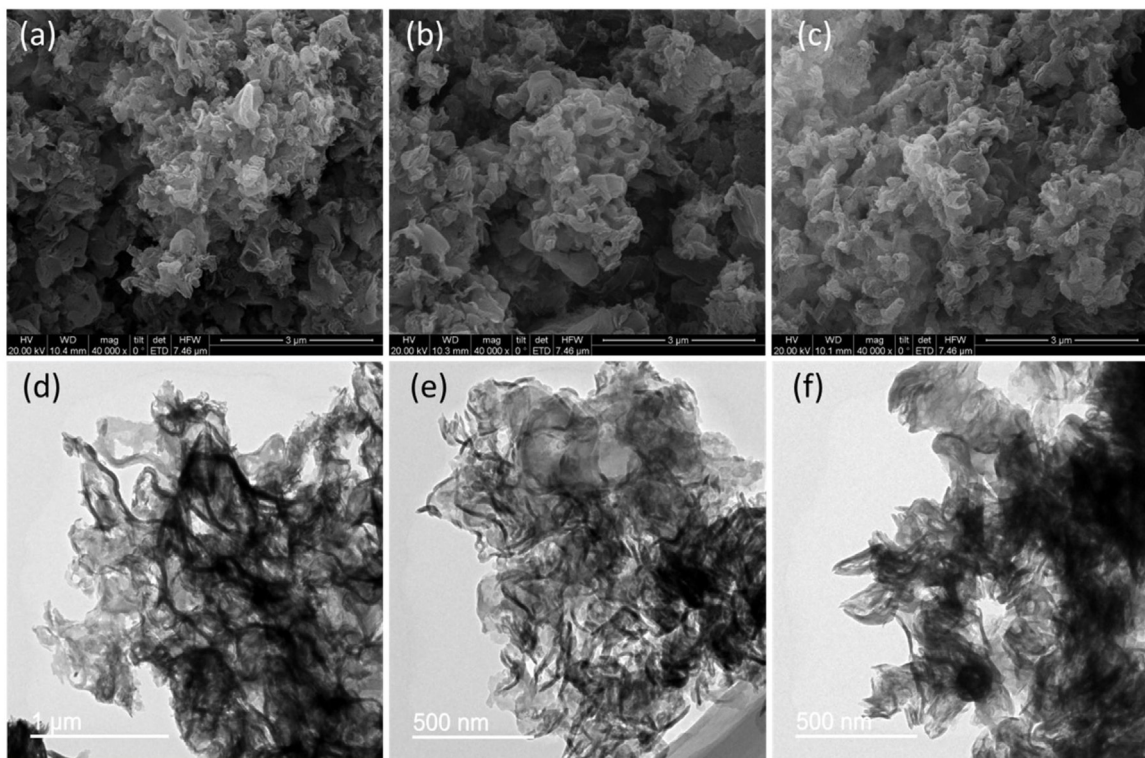


**Fig. 3.** SEM (a, b, c) and TEM images (d, e, f) of CN (a, d), 0.1KOH-CN (b, e) and 1.0 KOH-CN (c, f).

**Table 1**BET surface areas of g-C<sub>3</sub>N<sub>4</sub> and KOH decorated g-C<sub>3</sub>N<sub>4</sub> samples.

Sample	CN	0.05KOH-CN	0.1KOH-CN	0.25KOH-CN	0.5KOH-CN	1.0KOH-CN
BET surface area (m <sup>2</sup> /g)	61.9	61.6	62.4	59.0	62.2	59.1

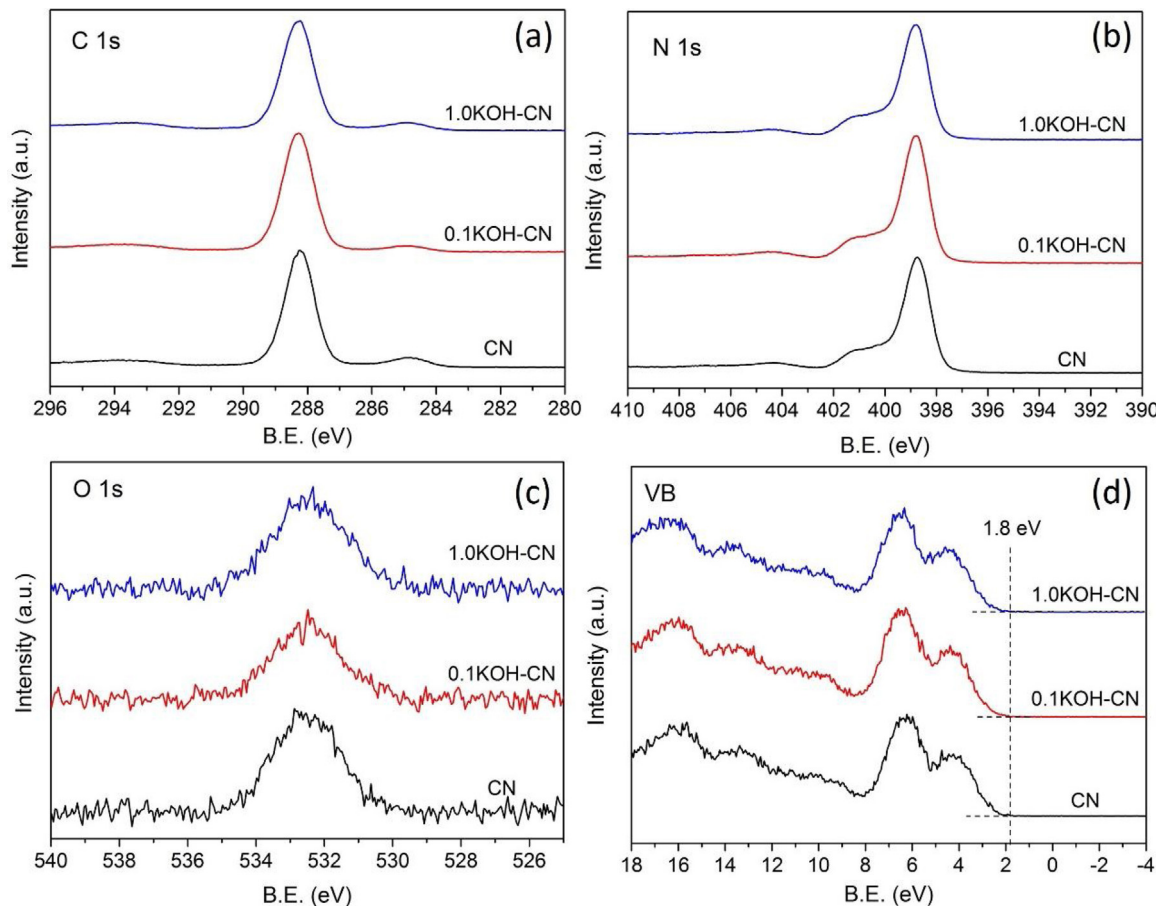


Fig. 4. C1s (a), N1s (b), O1s (c) and VB (d) XPS spectra of CN, 0.1KOH-CN and 1.0KOH-CN.

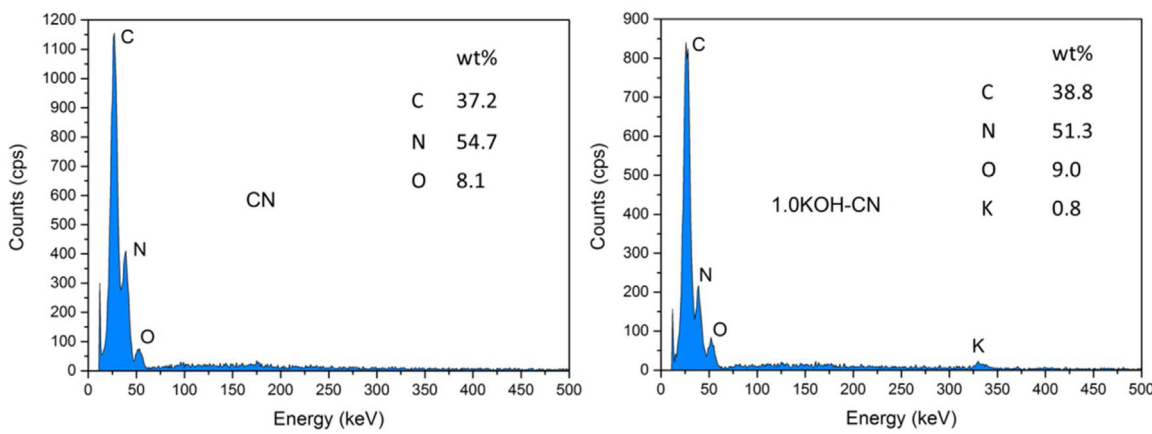


Fig. 5. SEM-EDX spectra of CN and 1.0KOH-CN.

### 3.3. Effect of anions

To clarify the role of KOH in enhancing the CO<sub>2</sub> reduction performance, we considered firstly if the cation K<sup>+</sup> could be responsible for the increase in CO<sub>2</sub> reduction and secondly whether the bicarbonates and/or carbonates (i.e. KHCO<sub>3</sub> and K<sub>2</sub>CO<sub>3</sub>) that formed

from reaction between KOH and CO<sub>2</sub> would participate in the catalytic process and facilitate the reactions. Therefore, CO<sub>2</sub> photocatalytic reduction performance of g-C<sub>3</sub>N<sub>4</sub> decorated with KOH (0.1 wt%), KCl (0.13 wt%), K<sub>2</sub>CO<sub>3</sub> (0.12 wt%) and KHCO<sub>3</sub> (0.18 wt%), respectively were further compared. The atomic ratio of K in each sample was kept the same. The results are illustrated in Fig. 9 and

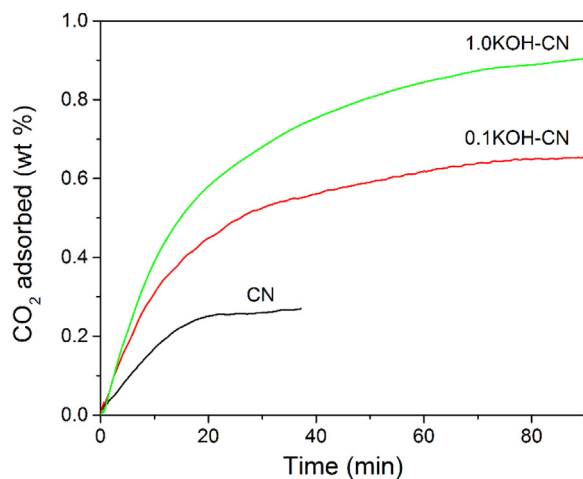


Fig. 6.  $\text{CO}_2$  absorption curves of CN, 0.1KOH-CN and 1.0KOH-CN at  $50^\circ\text{C}$ .

Fig. S2. Compared to the pristine CN, the samples loaded with KCl,  $\text{K}_2\text{CO}_3$  and  $\text{KHCO}_3$  show no improvement in CO or  $\text{CH}_4$  production and the yields of  $\text{CH}_3\text{CHO}$  over them become even inferior to that of CN. The results indicate that  $\text{K}^+$  alone is not able to promote the reactions, and that neither  $\text{KHCO}_3$  nor  $\text{K}_2\text{CO}_3$  would promote the conversion of  $\text{CO}_2$ .

When focusing on the first 100-min productions of CO and  $\text{CH}_4$ , as shown in Fig. S3 (d) and (e), it is found that  $\text{KHCO}_3$ -CN shows superior  $\text{CH}_4$  production to that of CN in the first 100 min. However, the influence does not last, and final productions in 5 h over  $\text{KHCO}_3$ -CN are poor. This suggests that  $\text{HCO}_3^-$  could be an adsorbed species that contributed to  $\text{CH}_4$  formation, but could not influence the  $\text{CO}_2$  adsorption or reduction significantly. All of these suggest that the existence of  $\text{OH}^-$  along with its high alkalinity is indispensable for the enhancement in  $\text{CO}_2$  photocatalytic reduction with KOH-CN.

#### 3.4. Effect of cations

Fig. 10 and Fig. S3 exhibit the accumulated and time-resolved product yields respectively in  $\text{CO}_2$  photocatalytic reduction over  $\text{g-C}_3\text{N}_4$  loaded with different amounts of NaOH with a comparison with those of CN and 0.1KOH-CN. NaOH-CN presents enhanced activity compared to CN as well. However, the optimal loading amount of NaOH is 1.0 wt%, which is 10 times larger than that of KOH. In addition, although the optimal  $\text{CH}_3\text{CHO}$  yields on 1.0NaOH-CN and 0.1KOH-CN are very close, the production of CO and  $\text{CH}_4$

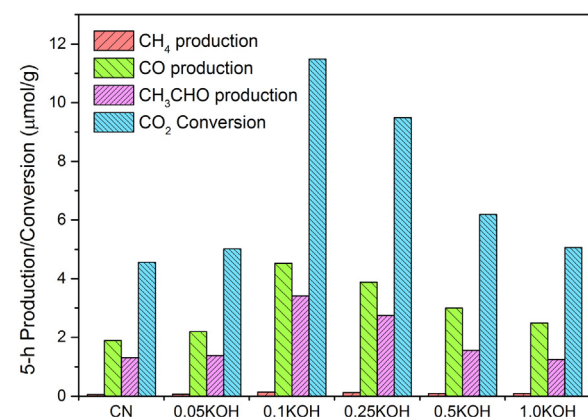


Fig. 8. 5-h production of CO,  $\text{CH}_4$  and  $\text{CH}_3\text{CHO}$  and conversion of  $\text{CO}_2$  over CN and CN decorated with different amount of KOH (denoted as  $x\text{KOH}$ ,  $x = 0.05, 0.1, 0.25, 0.5$  and  $1.0$ ) in photocatalytic  $\text{CO}_2$  reduction under visible light irradiation ( $\lambda > 420\text{ nm}$ ).

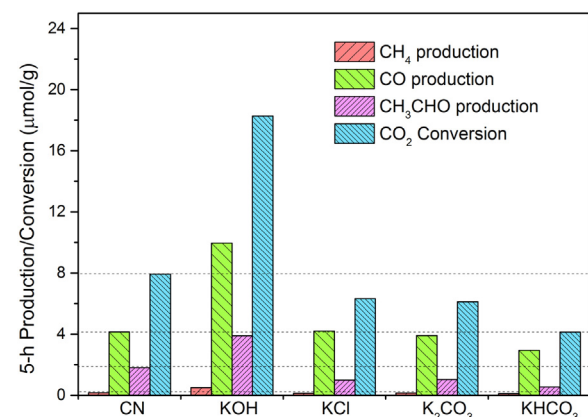


Fig. 9. 5-h production of CO,  $\text{CH}_4$  and  $\text{CH}_3\text{CHO}$  and conversion of  $\text{CO}_2$  over CN and CN loaded with KOH, KCl,  $\text{K}_2\text{CO}_3$  and  $\text{KHCO}_3$  respectively in photocatalytic  $\text{CO}_2$  reduction under irradiation of Xeon lamp.

over the best KOH-CN is about 1.5 times that of the best NaOH-CN. This implies that the characteristics of the cation are also important to determine the influence of the alkali on the photocatalyst ( $\text{g-C}_3\text{N}_4$ ).

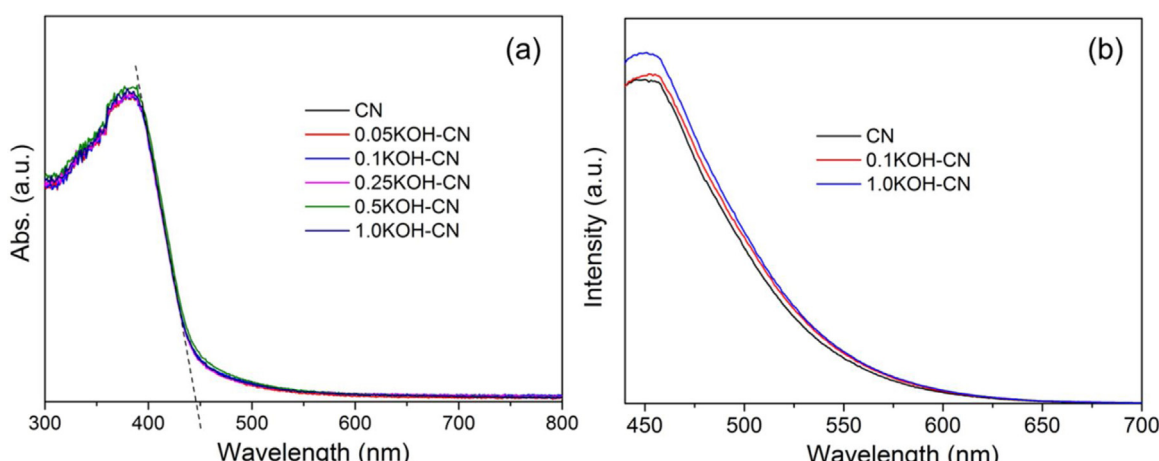
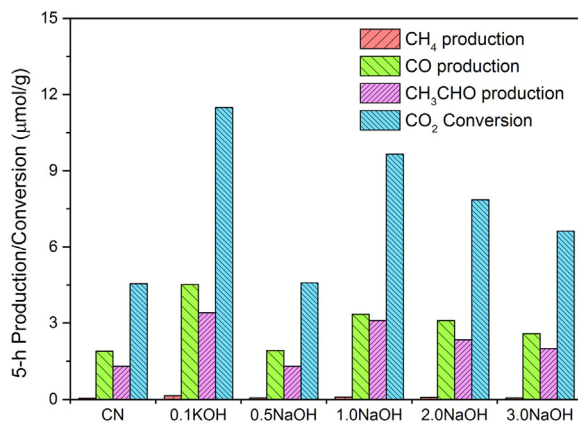
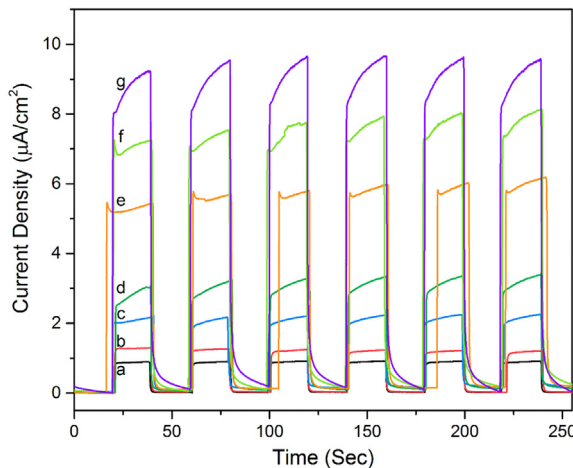


Fig. 7. UV-vis diffraction spectra of CN and CN with various KOH loading amount (a) and PL spectra of CN, 0.1KOH-CN and 1.0KOH-CN (b).



**Fig. 10.** 5-h production of CO, CH<sub>4</sub> and CH<sub>3</sub>CHO and conversion of CO<sub>2</sub> over Cn decorated with different amount of NaOH (denoted as xNaOH-CN, x=0.5, 1.0, 2.0 and 3.0) in photocatalytic CO<sub>2</sub> reduction under visible light irradiation ( $\lambda > 420$  nm) compared with 0.1KOH-CN (denoted as 0.1KOH) and CN.



**Fig. 11.** Photocurrent of g-C<sub>3</sub>N<sub>4</sub> at different pH values (the pH of a–f are tuned by KOH: a–pH 8.64; b–pH 9.55; c–pH 11.29; d–pH 12.35; e–pH 13.09; f–pH 13.59; the pH of g is tuned by NaOH: g–pH 13.58).

### 3.5. Discussion on the roles of KOH

Firstly, it is possible that OH<sup>–</sup> on g-C<sub>3</sub>N<sub>4</sub> functions as a hole scavenger and helps enhance the separation of photo-generated charges and thus the CO<sub>2</sub> conversion efficiency [43,53]. To verify this point, photocurrents of urea-polymerized g-C<sub>3</sub>N<sub>4</sub> at Na<sub>2</sub>SO<sub>4</sub> solution of different pH values tuned by KOH or NaOH were obtained, as presented in Fig. 11. The photocurrent increases significantly as the pH value rises, suggesting OH<sup>–</sup> can accept the photo-generated holes and suppress the recombination rate of the photo-excited charges. However, it is also found that the photocurrent of g-C<sub>3</sub>N<sub>4</sub> in Na<sub>2</sub>SO<sub>4</sub> solution with a pH of 13.59 adjusted by KOH is lower than that in Na<sub>2</sub>SO<sub>4</sub> solution with a pH of 13.58 adjusted by NaOH. In this light, if the improvement in CO<sub>2</sub> photocatalytic reduction is predominantly due to the role of OH<sup>–</sup> as a hole acceptor, the performance of KOH-CN and NaOH-CN should be close to each other, with NaOH possibly showing a greater promotion. But this is in contradiction with our observation that NaOH-CN has a lower enhancement in CO<sub>2</sub> reduction and a 10 times higher optimal loading than that of KOH-CN. Therefore, it can be deduced that there should be other factor(s) influencing the performance of the alkali-decorated g-C<sub>3</sub>N<sub>4</sub>.

Secondly, studies on the photochemical reduction [2,8,54,55] of CO<sub>2</sub> adsorbed in water, suggest that H<sub>2</sub>CO<sub>3</sub> and dissolved CO<sub>2</sub>

are highly likely to be the reactive species. As KOH and NaOH are deliquescent, a thin layer of alkaline electrolyte is expected to form on the surface of alkali decorated g-C<sub>3</sub>N<sub>4</sub> in the present water vapor and CO<sub>2</sub> [52]. The equilibria of CO<sub>2</sub> in water and basic solution are:



Since HCO<sub>3</sub><sup>–</sup> and CO<sub>3</sub><sup>2–</sup> showed little improvement in the catalytic performance, it is supposed that the main carbon-containing species involved in the alkali-enhanced reduction are H<sub>2</sub>CO<sub>3</sub> and dissolved CO<sub>2</sub>. Meanwhile, according to our calculation, the adsorption of CO<sub>2</sub> on g-C<sub>3</sub>N<sub>4</sub> cannot be influenced by the decoration of K<sup>+</sup> or Na<sup>+</sup> while the binding energy between H<sub>2</sub>CO<sub>3</sub> will be effected by K<sup>+</sup> and Na<sup>+</sup> with different extents. (More detailed information will be given in section 3.6) This implies that H<sub>2</sub>CO<sub>3</sub> is more likely to be main form of CO<sub>2</sub> that is reduced during the photocatalytic process. A recent work [55] studied the change of carbon species in various electrolytes after bubbling CO<sub>2</sub> and found that after bubbling with CO<sub>2</sub>, the ratio of H<sub>2</sub>CO<sub>3</sub> to the total carbon-species (i.e. H<sub>2</sub>CO<sub>3</sub>, CO<sub>2</sub>, HCO<sub>3</sub><sup>–</sup> and CO<sub>3</sub><sup>2–</sup>) in a low initial concentration of KOH (0.1 M) was higher than that in KHCO<sub>3</sub> (0.1 M). But this value would decrease dramatically if the concentration of KOH increased. In light of this, a low amount of OH<sup>–</sup>, as on our KOH decorated sample, may be able to keep a dynamically stable amount of H<sub>2</sub>CO<sub>3</sub> in the thin layer of solution on the catalyst's surface. Subsequently, the photocatalytic process with OH<sup>–</sup> as hole scavengers would consume the stabilized H<sub>2</sub>CO<sub>3</sub> before it changes to HCO<sub>3</sub><sup>–</sup> or CO<sub>3</sub><sup>2–</sup>. Thus, a formation-consumption cycle of H<sub>2</sub>CO<sub>3</sub> could be realized. In other words, a cycle of H<sub>2</sub>CO<sub>3</sub> generation, photocatalytic conversion and re-generation can be achieved with the relatively low amount of OH<sup>–</sup>. However, when the concentration of OH<sup>–</sup> is too high, the balance of H<sub>2</sub>CO<sub>3</sub> could be destroyed as the driving force to convert this species to HCO<sub>3</sub><sup>–</sup> and CO<sub>3</sub><sup>2–</sup> would be overwhelmed. Besides, a larger amount of alkali on the photocatalyst surface would also inhibit the transfer of photo-excited charges from g-C<sub>3</sub>N<sub>4</sub> to the reactive species [55].

With regard to the initial enhancement of CH<sub>4</sub> production with KHCO<sub>3</sub>-CN observed in Fig. S3, it could be explained by the fact that in the thin layer of electrolyte for the deliquescing of KHCO<sub>3</sub>, HCO<sub>3</sub><sup>–</sup> would coexist with H<sub>2</sub>CO<sub>3</sub> through Eq. (3). And the H<sub>2</sub>CO<sub>3</sub> would participate in the reactions when the samples are irradiated. However, KHCO<sub>3</sub> shows far less ability in adsorbing water and would form less amount of electrolyte. More essentially, the system with KHCO<sub>3</sub> lacks OH<sup>–</sup> as both a driving force for enhanced CO<sub>2</sub> adsorption and a hole acceptor. As a result, KHCO<sub>3</sub>-CN does not show apparent enhancement compared to bare g-C<sub>3</sub>N<sub>4</sub> over a long period.

### 3.6. Difference between sodium and potassium on alkali-decorated g-C<sub>3</sub>N<sub>4</sub>

In order to understand the difference between K (KOH) and Na (NaOH) in interacting with reducible CO<sub>2</sub> species on g-C<sub>3</sub>N<sub>4</sub>, density functional theory (DFT) calculations were performed with bare g-C<sub>3</sub>N<sub>4</sub> nanosheet and g-C<sub>3</sub>N<sub>4</sub> sheet with one K/Na atom. The plain g-C<sub>3</sub>N<sub>4</sub> nanosheet in calculation is corrugated g-C<sub>3</sub>N<sub>4</sub> sheet, as exhibited in the experimental section (Fig. 1a). The most stable forms of Na/g-C<sub>3</sub>N<sub>4</sub> and K/g-C<sub>3</sub>N<sub>4</sub> are presented in Fig. 12. Na/g-C<sub>3</sub>N<sub>4</sub> is with Na sitting most stably in the middle pore of the melon units, nearly in-plane with the g-C<sub>3</sub>N<sub>4</sub> sheet for its small atomic radius, whereas the most stable site for K atom on g-C<sub>3</sub>N<sub>4</sub> is on top of the whole above the g-C<sub>3</sub>N<sub>4</sub> plane. Meanwhile, both Na and K are

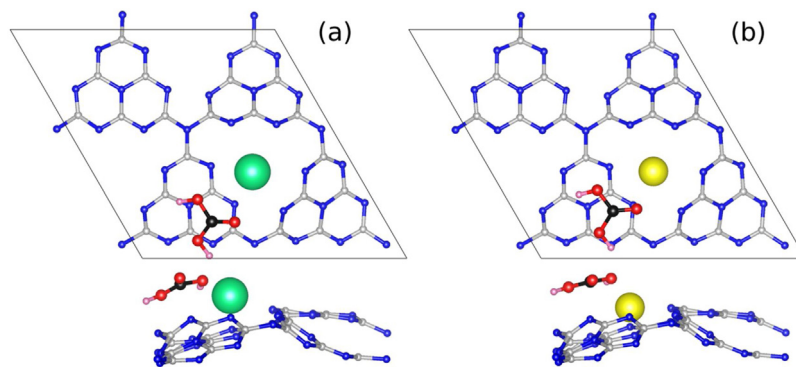


**Fig. 12.** Most stable adsorption sites for  $\text{H}_2\text{CO}_3$  on  $\text{g-C}_3\text{N}_4$  with K (a) and Na (b). (Grey, black – carbon atoms, blue – nitrogen atoms, red – oxygen atoms, pink – hydrogen atoms, green – potassium atoms and yellow – sodium atoms). (For interpretation of the references to colour in this figure legend, the reader is referred to the web version of this article.)

cationic on the sheet, i.e. are presenting as  $\text{Na}^+$  and  $\text{K}^+$ , according to the charge density differences results.

According to our calculation results, for  $\text{CO}_2$  adsorption on plain corrugated  $\text{g-C}_3\text{N}_4$  sheet, the binding energy is 0.25 eV. The most stable  $\text{CO}_2$  adsorption site is on top of the large tri-s-triazine pore and the interaction is considered to be physisorption because there is no change in the bond length of the C–O bond (1.18 Å). However, neither the addition of K nor Na on  $\text{g-C}_3\text{N}_4$  changes the binding energy of  $\text{CO}_2$  (0.25 eV).

While substituting  $\text{CO}_2$  with  $\text{H}_2\text{CO}_3$ , the situation becomes interestingly different. While the binding energy of  $\text{H}_2\text{CO}_3$  on the bare  $\text{g-C}_3\text{N}_4$  is 0.76 eV, it is 1.13 eV for K/ $\text{g-C}_3\text{N}_4$  and 0.86 eV for Na/ $\text{g-C}_3\text{N}_4$ . This change of  $\text{H}_2\text{CO}_3$  binding energy before and after the presence of K and Na can be regarded as an indirect indication that  $\text{H}_2\text{CO}_3$  is the main reduced  $\text{CO}_2$  species. And that the binding energy of  $\text{H}_2\text{CO}_3$  on K/ $\text{g-C}_3\text{N}_4$  was 31% larger than that on Na/ $\text{g-C}_3\text{N}_4$  could be one of the causes that why NaOH shows lower promotion effect to the  $\text{CO}_2$  photocatalytic reduction performance of  $\text{g-C}_3\text{N}_4$ .

Further investigations were carried out to find the reasons why the binding energy of  $\text{H}_2\text{CO}_3$  changes differently on K/ $\text{g-C}_3\text{N}_4$  and Na/ $\text{g-C}_3\text{N}_4$ . One reason could be the different preferred positions of  $\text{K}^+$  and  $\text{Na}^+$  on the  $\text{g-C}_3\text{N}_4$  sheet. As mentioned earlier, Na stays nearly in-plane with the  $\text{g-C}_3\text{N}_4$  sheet while K is out of the pore. Therefore, it is easier for the  $\text{H}_2\text{CO}_3$  to coordinate with K than Na. In another word, there is more steric hindrance for the interaction of  $\text{H}_2\text{CO}_3$  with the Na/ $\text{g-C}_3\text{N}_4$ . The other reason could be the possibly different electron densities in the sheet with K and that with Na. Fig. 13 exhibits the charge density difference for Na/ $\text{g-C}_3\text{N}_4$  and K/ $\text{g-C}_3\text{N}_4$ , which is obtained by subtraction the charge density of the separated species (K or Na and  $\text{g-C}_3\text{N}_4$ ) from the charge density of the complex. Both K and Na are cationic with higher electron density on the sheet near the ions. The charge density differences of the sheets with either of the atoms are nearly identical, except in the charge depleted region around the alkali metal atom itself. A larger area is shown around K than around Na. That is, when K is present, there is a larger region where  $\text{H}_2\text{CO}_3$  can be stabilized. In addition, little change in adsorption energy of  $\text{H}_2\text{CO}_3$  on local minimum energy sites away from the K/Na ion is found, suggesting that the additional electrons in the unit cell of  $\text{g-C}_3\text{N}_4$  won't influence the adsorption of  $\text{H}_2\text{CO}_3$ . It is only  $\text{K}^+$  and  $\text{Na}^+$  that are responsible for the enhanced stabilization of  $\text{H}_2\text{CO}_3$ .

For  $\text{g-C}_3\text{N}_4$  samples synthesized by polymerization of a certain precursor, there are always residual hydrogens connected to the nitrogen due to incomplete condensation [20]. Therefore, we further calculated the adsorption energy of  $\text{H}_2\text{CO}_3$  on the  $\text{g-C}_3\text{N}_4$  system containing -NH (Fig. 1b) and an enhanced adsorption was observed compared to the pure  $\text{g-C}_3\text{N}_4$  sheet. The binding energy

for  $\text{H}_2\text{CO}_3$  on  $\text{g-C}_3\text{N}_4$  with -NH is 1.08 eV and the molecule will sit in the pore with -NH groups. The increased binding energy is supposed to be originated from the hydrogen bonding between the adsorbate and the sheet.

When adding K/Na to the  $\text{g-C}_3\text{N}_4$  sheet with some pores containing -NH groups while the others not, it is found that K and Na prefer to bind to a pore without -NH. The binding energies of alkali-metal atoms on the pores of the pure sheet are 3.47 eV and 3.64 eV for K and Na respectively. While, on the pores adjacent to -NH bond in the -NH containing sheet, the binding energy of K is only 3.20 eV and Na 3.57 eV. Therefore, both metals, especially K, would prefer to sit on sections of the material that are far away from the pores containing -NH. In this light, the reduced promoting effect of KOH when excessive amount of KOH is decorated could also be explained by the fact that K selectively adsorbs on the pores without -NH and only as its concentration increases to a certain value would it also adsorb to pores adjacent to -NH and reduces the adsorption energy of the reaction intermediate,  $\text{H}_2\text{CO}_3$ , in the pore with the -NH bonds to 0.95 eV. In contrast, the adsorption of Na is less selective between the pores adjacent to -NH groups and the clean ones, but it would also weaken the binding energy of  $\text{H}_2\text{CO}_3$  in the hydrogen-containing  $\text{g-C}_3\text{N}_4$  (from 1.08 eV to 0.94 eV). Therefore, it could be concluded that both the lower enhancement to the adsorption of  $\text{H}_2\text{CO}_3$  on clean  $\text{g-C}_3\text{N}_4$  and the poorer selectivity to favorable sitting sites on -NH contained  $\text{g-C}_3\text{N}_4$  contribute to the inferior promoting effect of NaOH on  $\text{g-C}_3\text{N}_4$  for  $\text{CO}_2$  photocatalytic reduction compared to KOH.

### 3.7. Deactivation of the catalyst

Deactivation during the  $\text{CO}_2$  photocatalytic reduction process is very common for various materials, including  $\text{TiO}_2$  [6],  $\text{Bi}_2\text{WO}_6$  [13],  $\text{ZnGeO}_4$  [56], and  $\text{g-C}_3\text{N}_4$  [52] etc., due to inhibited desorption of some intermediates and enhanced back reaction with the formation of oxygen [6]. The deactivation of  $\text{g-C}_3\text{N}_4$  was also observed in this work. As presented in Fig. 14, the evolution rate of the products ( $\text{CO}$ ,  $\text{CH}_4$  and  $\text{CH}_3\text{CHO}$ ) on pristine  $\text{g-C}_3\text{N}_4$  (CN) increased in the first hour and then decreased gradually. Decorating KOH onto  $\text{g-C}_3\text{N}_4$  as a strategy to enhance  $\text{CO}_2$  reduction might be expected to exacerbate this problem as KOH could change to  $\text{KHCO}_3$  or  $\text{K}_2\text{CO}_3$  during the reaction. However, comparing the activity change of CN and 0.1K-CN as presented in Fig. 14, the drop of photocatalytic efficiency with 0.1KOH-CN is even slower than that with CN, suggesting that the chemical change of KOH on  $\text{g-C}_3\text{N}_4$  could not be dramatic.

To analyze this further, DRIFTS experiments were carried out on 0.1KOH-CN. Using the pre-treated 0.1KOH-CN surface in helium at 50 °C as a background, the in-situ DRIFT spectrum of 0.1KOH-CN after 60-min adsorption of  $\text{CO}_2$  and  $\text{H}_2\text{O}$  and a further 30-min

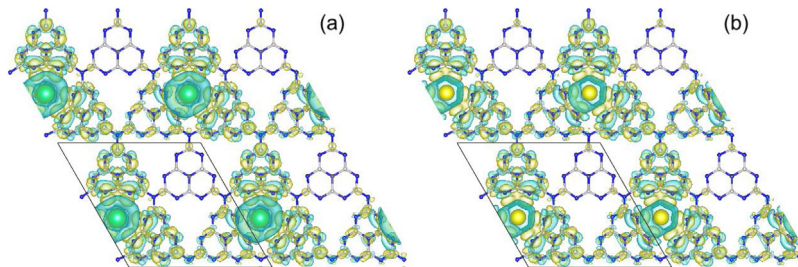


**Fig. 13.** Charge density differences with K (a) and Na (b) on g-C<sub>3</sub>N<sub>4</sub>. (Iso-level of 0.0008 e/bohr<sup>3</sup>; Grey – carbon atoms, blue – nitrogen atoms, green – potassium atoms and yellow – sodium atoms; Charge depletion in aqua and accumulation in yellow; Box shows the size of the super cell). (For interpretation of the references to colour in this figure legend, the reader is referred to the web version of this article.)

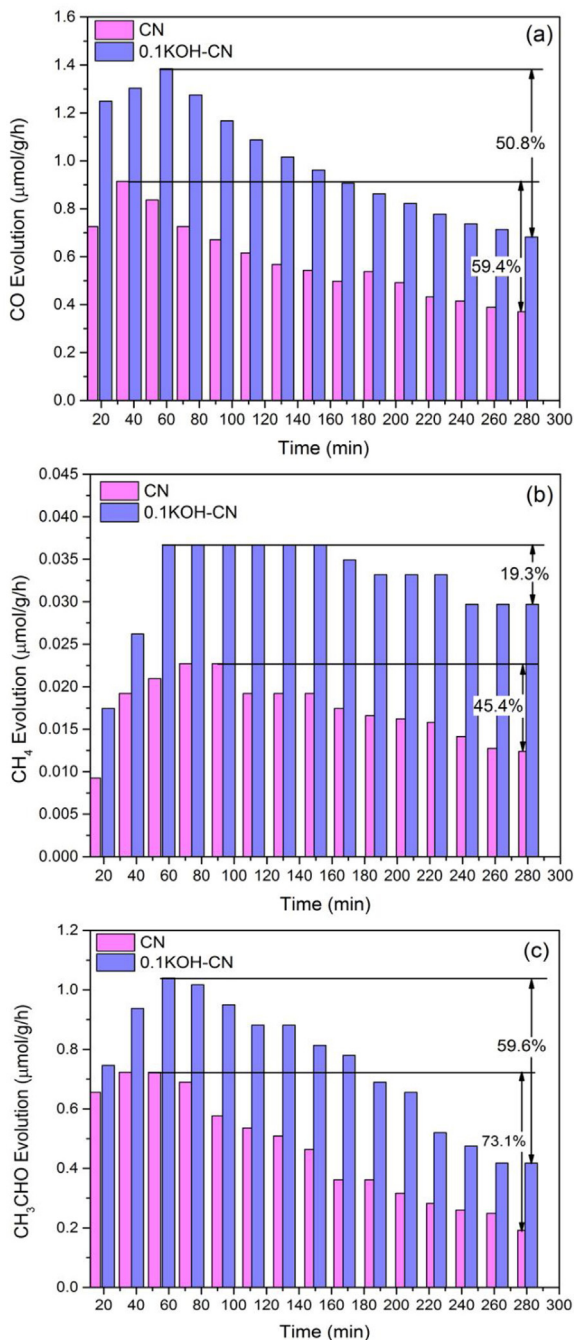


**Fig. 14.** Time-course evolutions of CO (a), CH<sub>4</sub> (b) and CH<sub>3</sub>CHO (c) over CN and 0.1KOH-CN.

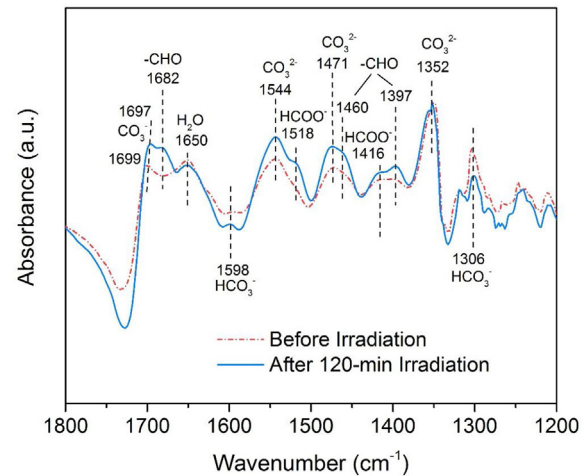


**Fig. 15.** In-situ DRIFT spectra of 0.1KOH-CN with adsorbed forms of H<sub>2</sub>O and CO<sub>2</sub>: before irradiation and after 120-min light irradiation.

He purging is presented in Fig. 15 along with the spectrum of the adsorbed surface after 120-min light irradiation. After the adsorption of CO<sub>2</sub> and H<sub>2</sub>O, besides the adsorption peak of H<sub>2</sub>O at 1650 cm<sup>-1</sup>, the absorption peaks of HCO<sub>3</sub><sup>-</sup> and CO<sub>3</sub><sup>2-</sup> are apparent at 1598, 1306 cm<sup>-1</sup> and 1699, 1544, 1352 cm<sup>-1</sup>, respectively [21,40], indicating that KOH has been partially converted to KHCO<sub>3</sub> and K<sub>2</sub>CO<sub>3</sub> before the photocatalytic reactions. After 120-min irradiation, the absorbance of HCO<sub>3</sub><sup>-</sup> shows a certain decrease whereas the peaks attributed to CO<sub>3</sub><sup>2-</sup> either remain or increase. Meanwhile, new absorptions of formate (-HCOO<sup>-</sup>) (1518, 1416 cm<sup>-1</sup>) and formaldehyde (-CHO) (1682, 1460, 1397 cm<sup>-1</sup>) from the intermediates in CO<sub>2</sub> photocatalytic reduction [21,57,58] appear. Note, the CO<sub>3</sub><sup>2-</sup> peaks that show increase in intensity are close to these new peaks, so their increase could be at least partially attributed to their overlap with the new peaks. Overall, the total amount of HCO<sub>3</sub><sup>-</sup> and CO<sub>3</sub><sup>2-</sup> does not show much difference before and after irradiation, validating the robustness of the effect of KOH on g-C<sub>3</sub>N<sub>4</sub>.

#### 4. Conclusion

In this work, we reported the remarkably improved photocatalytic activity of CO<sub>2</sub> reduction over KOH-decorated g-C<sub>3</sub>N<sub>4</sub> compared to pristine g-C<sub>3</sub>N<sub>4</sub>. In the thin layer of alkaline electrolyte formed on the surface of g-C<sub>3</sub>N<sub>4</sub> due to the high deliquescence of KOH, OH<sup>-</sup> not only functions as a hole acceptor, but also keeps the formation and consumption cycle of H<sub>2</sub>CO<sub>3</sub> (the most likely form of CO<sub>2</sub> to be reduced). In addition, it was found that the promotion effect of KOH was much more obvious than NaOH. Though DFT calculation, the reasons turned out to contain that (1) while both K<sup>+</sup> and Na<sup>+</sup> are able to enhance the binding of H<sub>2</sub>CO<sub>3</sub> on clean

g-C<sub>3</sub>N<sub>4</sub> pores, the influence of K<sup>+</sup> is much stronger; and (2) for commonly synthesize g-C<sub>3</sub>N<sub>4</sub> with –NH<sub>x</sub>, K<sup>+</sup>/Na<sup>+</sup> located adjacent to the pore with –NH would impair the adsorption of H<sub>2</sub>CO<sub>3</sub> but K<sup>+</sup> showed a higher selectivity to staying at the sites far away from the –NH-containing pores. Furthermore, the robustness of the effect of KOH on g-C<sub>3</sub>N<sub>4</sub> during the photocatalytic process was verified. The findings provide insights into the mechanism of CO<sub>2</sub> photocatalytic reduction on alkali-modified photocatalysts, and should inspire development of efficient photocatalysts for CO<sub>2</sub> photocatalytic reduction.

## Acknowledgments

We acknowledge the financial supports of the Natural Science Foundation of Zhejiang Province (No. Z5100116), National Natural Science Foundation of China (No. 51578488), Changjiang Scholar Program of Chinese Ministry of Education (China, 2009). We thank the Australian Research Council for support of this project through the DP and LIEF programs. This research was undertaken with the assistance of resources provided at the NCI National Facility systems at the Australian National University through the National Computational Merit Allocation Scheme supported by the Australian Government with support from the Queensland Cyber Infrastructure Foundation (QCIF) and the University of Queensland Research Computing Centre. J.M.T.A.F. thanks the University of Queensland for the UQI scholarships supporting her Ph.D.

## Appendix A. Supplementary data

Supplementary data associated with this article can be found, in the online version, at <http://dx.doi.org/10.1016/j.apcatb.2017.05.064>.

## References

- [1] T. Inoue, A. Fujishima, S. Konishi, K. Honda, *Nature* 277 (1979) 637–638.
- [2] S.N. Habisreutinger, L. Schmidt-Mende, J.K. Stolarczyk, *Angew. Chem. Int. Ed.* 52 (2013) 7372–7408.
- [3] M. Mikkelsen, M. Jorgensen, F.C. Krebs, *Energy Environ. Sci.* 3 (2010) 43–81.
- [4] S. Navalón, A. Dhakshinamoorthy, M. Álvaro, H. García, *ChemSusChem* 6 (2013) 562–577.
- [5] M. Tahir, N.S. Amin, *Energy Convers. Manage.* 76 (2013) 194–214.
- [6] W. Tu, Y. Zhou, Z. Zou, *Adv. Mater.* 26 (2014) 4607–4626.
- [7] S. Ye, R. Wang, M.-Z. Wu, Y.-P. Yuan, *Appl. Surf. Sci.* 358 (2015) 15–27.
- [8] K. Li, B.S. Peng, T.Y. Peng, *ACS Catal.* 6 (2016) 7485–7527.
- [9] A.D. Handoko, J. Tang, *Int. J. Hydrogen Energy* 38 (2013) 13017–13022.
- [10] Y. Wang, F. Wang, Y. Chen, D. Zhang, B. Li, S. Kang, X. Li, L. Cui, *Appl. Catal. B* 147 (2014) 602–609.
- [11] P. Li, Y. Zhou, Z. Zhao, Q. Xu, X. Wang, M. Xiao, Z. Zou, *J. Am. Chem. Soc.* 137 (2015) 9547–9550.
- [12] K. Li, A.D. Handoko, M. Khraisheh, J. Tang, *Nanoscale* 6 (2014) 9767–9773.
- [13] Z. Sun, Z. Yang, H. Liu, H. Wang, Z. Wu, *Appl. Surf. Sci.* 315 (2014) 360–367.
- [14] T. Baran, S. Wojtyła, A. Dibenedetto, M. Aresta, W. Macyk, *Appl. Catal. B* 178 (2015) 170–176.
- [15] J. Chen, S. Qin, G. Song, T. Xiang, F. Xin, X. Yin, *Dalton Trans.* 42 (2013) 15133–15138.
- [16] H.-C. Hsu, I. Shown, H.-Y. Wei, Y.-C. Chang, H.-Y. Du, Y.-G. Lin, C.-A. Tseng, C.-H. Wang, L.-C. Chen, Y.-C. Lin, K.-H. Chen, *Nanoscale* 5 (2013) 262–268.
- [17] H. Wang, Z. Sun, Q. Li, Q. Tang, Z. Wu, *J. CO<sub>2</sub> Util.* 14 (2016) 143–151.
- [18] S. Cao, J. Low, J. Yu, M. Jaroniec, *Adv. Mater.* 27 (2015) 2150–2176.
- [19] A. Thomas, A. Fischer, F. Goettmann, M. Antonietti, J.-O. Müller, R. Schlogl, J.M. Carlsson, *J. Mater. Chem.* 18 (2008) 4893–4908.
- [20] W.-J. Ong, L.-L. Tan, Y.H. Ng, S.-T. Yong, S.-P. Chai, *Chem. Rev.* 116 (2016) 7159–7329.
- [21] P. Xia, B. Zhu, J. Yu, S. Cao, M. Jaroniec, *J. Mater. Chem. A* 5 (2017) 3230–3238.
- [22] Z. Zhao, Y. Sun, F. Dong, *Nanoscale* 7 (2015) 15–37.
- [23] N. Tian, H. Huang, C. Liu, F. Dong, T. Zhang, X. Du, S. Yu, Y. Zhang, *J. Mater. Chem. A* 3 (2015) 17120–17129.
- [24] Q. Zhang, H. Wang, S. Hu, G. Lu, J. Bai, X. Kang, D. Liu, J. Gui, *RSC Adv.* 5 (2015) 42736–42743.
- [25] B. Lin, G. Yang, B. Yang, Y. Zhao, *Appl. Catal. B* 198 (2016) 276–285.
- [26] S.-W. Cao, X.-F. Liu, Y.-P. Yuan, Z.-Y. Zhang, Y.-S. Liao, J. Fang, S.C.J. Loo, T.C. Sum, C. Xue, *Appl. Catal. B* 147 (2014) 940–946.
- [27] H. Shi, G. Chen, C. Zhang, Z. Zou, *ACS Catal.* 4 (2014) 3637–3643.
- [28] M. Li, L. Zhang, X. Fan, Y. Zhou, M. Wu, J. Shi, *J. Mater. Chem. A* 3 (2015) 5189–5196.
- [29] Y. Huang, M. Fu, T. He, *Acta Phys. Chim. Sin.* 31 (2015) 1145–1152.
- [30] Y. He, L. Zhang, B. Teng, M. Fan, *Environ. Sci. Technol.* 49 (2015) 649–656.
- [31] J.-C. Wang, H.-C. Yao, Z.-Y. Fan, L. Zhang, J.-S. Wang, S.-Q. Zang, Z.-J. Li, *ACS Appl. Mater. Interfaces* 8 (2016) 3765–3775.
- [32] M. Li, L. Zhang, X. Fan, M. Wu, M. Wang, R. Cheng, L. Zhang, H. Yao, J. Shi, *Appl. Catal. B* 201 (2017) 629–635.
- [33] Y. Wang, R. Shi, J. Lin, Y. Zhu, *Energy Environ. Sci.* 4 (2011) 2922–2929.
- [34] W. Yu, D. Xu, T. Peng, *J. Mater. Chem. A* 3 (2015) 19936–19947.
- [35] M. Li, L. Zhang, M. Wu, Y. Du, X. Fan, M. Wang, L. Zhang, Q. Kong, J. Shi, *Nano Energy* 19 (2016) 145–155.
- [36] H. Li, S. Gan, H. Wang, D. Han, L. Niu, *Adv. Mater.* 27 (2015) 6906–6913.
- [37] Q. Huang, J. Yu, S. Cao, C. Cui, B. Cheng, *Appl. Surf. Sci.* 358 (2015) 350–355.
- [38] L. Shi, T. Wang, H. Zhang, K. Chang, J. Ye, *Adv. Funct. Mater.* 25 (2015) 5360–5367.
- [39] L. Liu, C. Zhao, H. Zhao, D. Pitts, Y. Li, *Chem. Commun. (Camb)* 49 (2013) 3664–3666.
- [40] L. Liu, C. Zhao, D. Pitts, H. Zhao, Y. Li, *Catal. Sci. Technol.* 4 (2014) 1539–1546.
- [41] S. Xie, Y. Wang, Q. Zhang, W. Fan, W. Deng, Y. Wang, *Chem Commun (Camb)* 49 (2013) 2451–2453.
- [42] S. Xie, Y. Wang, Q. Zhang, W. Deng, Y. Wang, *ACS Catal.* 4 (2014) 3644–3653.
- [43] X. Meng, S. Ouyang, T. Kako, P. Li, Q. Yu, T. Wang, J. Ye, *Chem. Commun.* 50 (2014) 11517–11519.
- [44] G. Kresse, J. Furthmüller, *Phys. Rev. B* 54 (1996) 11169–11186.
- [45] J.P. Perdew, K. Burke, M. Ernzerhof, *Phys. Rev. Lett.* 77 (1996) 3865–3868.
- [46] S. Grimme, *J. Comput. Chem.* 27 (2006) 1787–1799.
- [47] M. Hankel, D. Ye, L. Wang, D.J. Searles, *J. Phys. Chem. C* 119 (2015) 21921–21927.
- [48] S.C. Yan, Z.S. Li, Z.G. Zou, *Langmuir* 25 (2009) 10397–10401.
- [49] F. Dong, L. Wu, Y. Sun, M. Fu, Z. Wu, S.C. Lee, *J. Mater. Chem.* 21 (2011) 15171–15174.
- [50] J. Liu, T. Zhang, Z. Wang, G. Dawson, W. Chen, *J. Mater. Chem.* 21 (2011) 14398–14401.
- [51] Y. Zhang, J. Liu, G. Wu, W. Chen, *Nanoscale* 4 (2012) 5300–5303.
- [52] J. Yu, K. Wang, W. Xiao, B. Cheng, *Phys. Chem. Chem. Phys.* 16 (2014) 11492–11501.
- [53] S. Sato, J.M. White, *J. Catal.* 69 (1981) 128–139.
- [54] B. Kumar, M. Llorente, J. Froehlich, T. Dang, A. Sathrum, C.P. Kubiak, *Annu. Rev. Phys. Chem.* 63 (2012) 541–569.
- [55] H. Zhong, K. Fujii, Y. Nakano, F. Jin, *J. Phys. Chem. C* 119 (2015) 55–61.
- [56] Q.Z. Liu, Y. Tian, Z.P. Chen, X.Y. Gao, J. Zou, Z.G., *J. Mater. Chem.*, 22 2012 2033–2038.
- [57] S.E. Collins, M.A. Baltanás, A.L. Bonivardi, *J. Catal.* 226 (2004) 410–421.
- [58] J. Araña, J.M. Doña-Rodríguez, C.G.i. Cabo, O. González-Díaz, J.A. Herrera-Melián, J. Pérez-Peña, *Appl. Catal. B* 53 (2004) 221–232.